Edelweiss Applied Science and Technology
ISSN: 2576-8484
Vol. 9, No. 8, 1084-1098
2025
Publisher: Learning Gate
DOI: 10.55214/2576-8484.v9i8.9555

Nonlinear behavior of reinforced concrete shear walls with various openings

Muhammad Maheswara Aryasatya[1], Made Sukrawa[2*], I Ketut Sudarsana[3], Putu Ryandika Putra[4]
[1,2,3,4]Civil Engineering, Udayana University, Badung, Bali, Indonesia; aryasatya.2205511013@student.unud.ac.id (M.M.A.). Msukrawa@unud.ac.id (M.S.) ksudarsana@unud.ac.id (I.K.S.) puturyandikaputra20@gmail.com (P.R.P.).

Abstract: This study analyzes the nonlinear behavior of reinforced concrete shear walls with openings using two-dimensional models in SAP2000. The analysis includes two main models—a full shear wall (MV-WS) and a shear wall with reinforced openings (MV-WO)—as well as eight variation models: four with different opening percentages (OV22, OV37, OV52, OV72) and four with varying opening positions (OS, OE18, OE36, OE54). The objective is to evaluate the use of layered shell elements for modeling shear walls with openings and to assess displacement and stress responses due to variations in opening size and location. Validation against experimental load–displacement curves and crack patterns confirmed that the layered shell approach captures elastic behavior effectively, although it is less accurate for plastic responses. The findings show that a lower percentage of openings leads to greater base shear capacity, and that shear strength improves with increased compressed area resulting from optimal opening placement.

Keywords: *3-5 shear wall, Pushover analysis, Validation model, Variation model.*

1. Introduction

Shear wall modeling has been extensively studied using both macro and micro approaches. Rezapour and Ghassemieh [1] enhanced the Multiple-Vertical Line Element Model (MVLEM) for coupled shear walls, finding macro-modeling to be 1000–2000 times faster than micro-modeling [1]. Similarly, Haghi, et al. [2] used macro-modeling for steel–concrete composite shear walls, showing that stiffness and peak shear strength increased with a lower aspect ratio, higher axial load, greater concrete strength (f'c), and reduced stud spacing. Vertical mesh discretization also provided better alignment with experimental data than horizontal discretization [2].

To enhance seismic performance, shear walls are commonly used to resist lateral forces during earthquakes. However, the inclusion of openings for doors or lobbies can compromise their structural integrity. Sivaguru and Rao [3] observed that shear strength could drop by up to 60% due to such openings, although the use of Fiber Reinforced Concrete (FRC) was shown to regain around 15% of that lost strength [3]. In this study, the finite element method (FEM) using SAP2000 software is applied to assess the impact of different opening sizes and locations on the behavior of shear walls. The models use two-dimensional layered shell elements to capture nonlinear responses, based on data from Sivaguru and Rao. The analysis focuses on displacement and stress distribution, with the goal of informing more effective seismic-resistant design strategies. Additionally, Kelly, et al. [4] as cited in Zhang et al. (2018), outlined three techniques for understanding load transfer: principal stress vectors, energy flow vectors, and finite element analysis [4].

2. Research Methods

2.1. Strength and Behavior of Shear Walls with Openings Under Cyclic Loading

Sivaguru and Rao [3] developed three shear wall models in their study: one representing a

History: Received: 19 June 2025; Revised: 5 August 2025; Accepted: 8 August 2025; Published: 20 August 2025
* Correspondence: Msukrawa@unud.ac.id

solid, unperforated wall (Exp-WS) and another representing a shear wall with openings (Exp-WO) [3].

2.2. Strength and Behavior of Shear Walls with Openings Under Cyclic Loading

According to the CSI Analysis Reference Manual for SAP2000 v.23, the layered shell feature enables shell elements to display nonlinear behavior by enforcing full composite action between layers. This nonlinearity specifically refers to material nonlinearity, which results from a non-linear stress-strain relationship—either within the elastic range or in the elasto-plastic or perfectly plastic regions. The material used in the layers can be isotropic, uniaxial, or orthotropic, and its nonlinear response depends on the properties of the materials chosen for each layer [5].

2.3. Pushover Analysis

Based on the Indonesian Earthquake Code SNI 1726-2019, pushover analysis is a type of nonlinear static analysis where earthquake effects are represented as static lateral loads applied at the center of mass on each floor. These loads are incrementally increased until initial yielding occurs—marked by the formation of plastic hinges—and continued until the structure reaches its target displacement or a plastic state [6]. According to Applied Technology Council (ATC) [7] the steps in pushover analysis involve developing a computer model of the structure, setting performance objectives, applying gravity loads along with a defined lateral load pattern, tracking displacement at a control point, and generating a capacity curve that illustrates the relationship between base shear and displacement at that point. While pushover analysis is a useful method for evaluating and designing earthquake-resistant structures, it also has limitations. These include its reliance on monotonic static loading, the need for accurate selection of lateral load patterns, and the complexity of modeling nonlinear behaviors such as inelastic deformations and P-Δ effects [7].

2.4. Structural Model Validation Data

The material specifications used for validating the model are based on the experimental work of Sivaguru and Rao [3]. In the MV-WS model, the concrete has a compressive strength of 24 MPa and a tensile strength of 3.1 MPa. For the MV-WO model, the compressive and tensile strengths are slightly higher, at 26 MPa and 3.3 MPa respectively. The top beam measures 300×400 mm and is reinforced with 4D-13 longitudinal bars and Ø10-100 stirrups, while the bottom beam is 500×600 mm with 6D-16 longitudinal bars and Ø10-100 stirrups. The MV-WO model includes an opening sized 300×700 mm, and the shear wall has a thickness of 125 mm. The columns are 300×150 mm and reinforced with 4D-12 longitudinal bars along with Ø8-100 stirrups [3]. In both the MV-WS and MV-WO web sections, two layers of 8 mm diameter reinforcement bars are placed in both directions at 200 mm spacing. For the MV-WO model, additional reinforcement is provided around the openings, consisting of 8 mm longitudinal bars spaced at 30 mm and 12 mm transverse bars also spaced at 30 mm [3].

Edelweiss Applied Science and Technology
ISSN: 2576-8484
Vol. 9, No. 8: 1084-1098, 2025
DOI: 10.55214/2576-8484.v9i8.9555

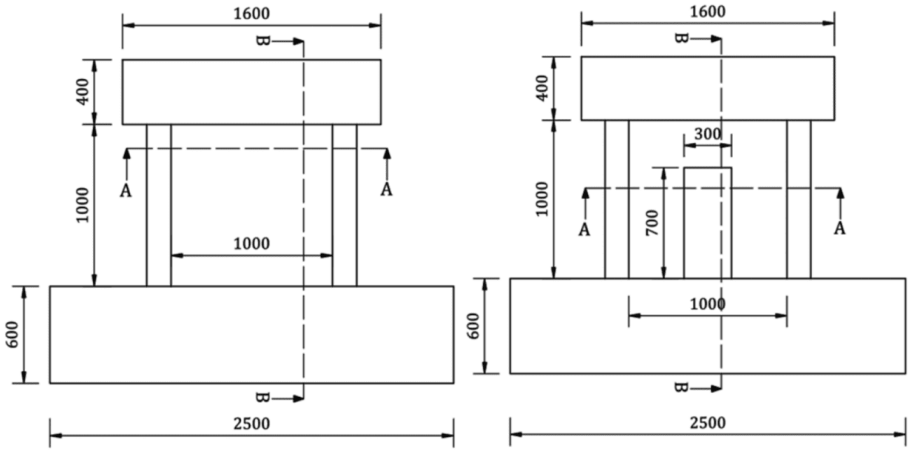

Figure 1.
Cross-sectional geometry of solid wall structure (left), and validation-wall (right).

The validation model was developed to assess the accuracy of the shear wall modeling approach by comparing it with experimental test results. A monotonic load was applied at the upper right corner of the beam–column joint, as illustrated in Figure 1 [3].

2.5. Modelling in SAP2000

A full shell model was used for all components since the test specimens were cast monolithically [8]. Beams, columns, and walls were assigned isotropic material properties, while reinforcement was modeled with uniaxial behavior [9]. The shear wall used concrete material, with its stress–strain curve input based on the *SAP2000 - 20 Nonlinear Shear Walls* tutorial by Computers and Structures, Inc.

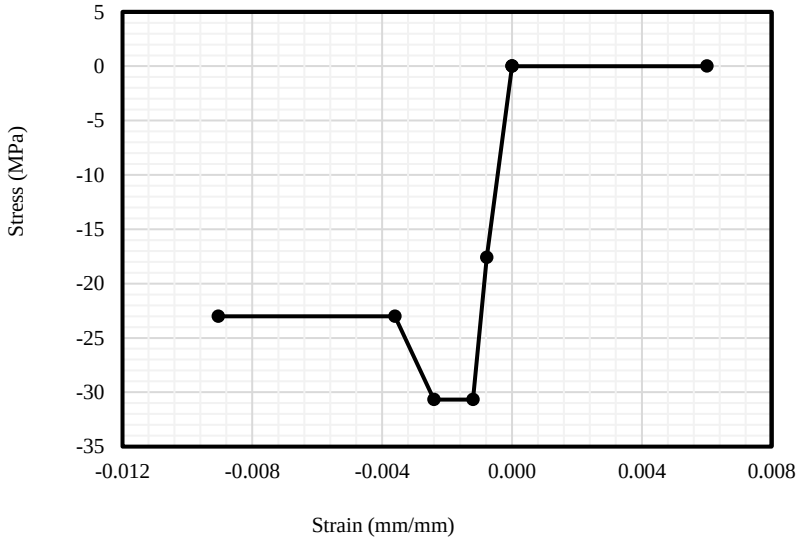

Figure 2.
Concrete stress-strain curve.

The concrete layer thickness was calculated by dividing the area of one reinforcement bar by its spacing [10]. Pushover analysis was then performed, with target displacements set at 22 mm for the

Edelweiss Applied Science and Technology
ISSN: 2576-8484
Vol. 9, No. 8: 1084-1098, 2025
DOI: 10.55214/2576-8484.v9i8.9555

validation model and 35 mm for the variation model. The analysis included two stages: first, applying gravity loads (dead loads with a factor of 1.0), followed by lateral pushover loading to simulate earthquake forces [6].

2.6. Model Variation Structural Data

The variation model uses the same material properties as MV-WO from Sivaguru and Rao (2021), but with modified geometry. The top beam is 400×600 mm with 4D-13 longitudinal and Ø10-100 stirrups, while the bottom beam is 500×600 mm with 4D-16 longitudinal and Ø10-100 stirrups. The web has two layers of 8 mm bars spaced at 200 mm in both directions, with additional reinforcement similar to MV-WO. The initial opening size is 2100×900 mm, and the study explores the impact of varying the size and position of these openings, as shown in Figure 3.

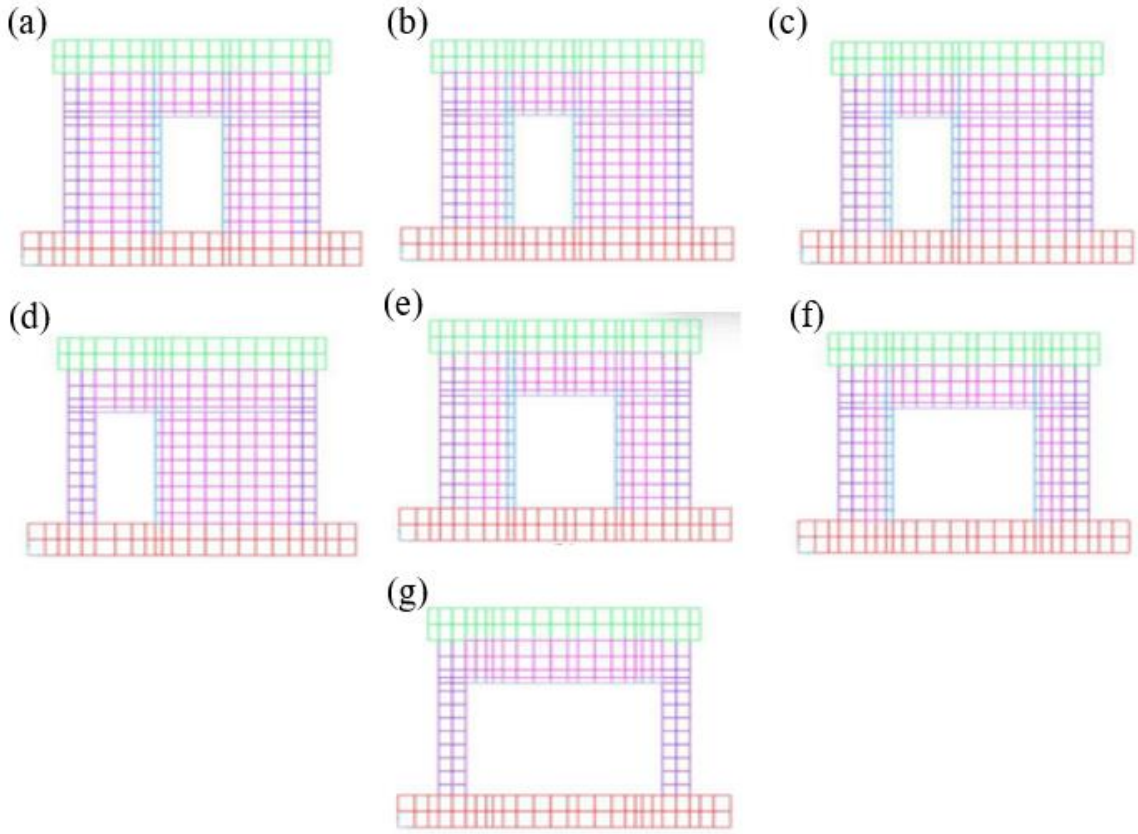

Figure 3.
Model variation (a) opening sentries (OS), (b) opening eccentricity 18% (OE18), (c) opening eccentricity 36% (OE36), (d) opening eccentricity 54% (OE54), (e) 37% opening variation (OV37), (f) 52% opening variation (OV52) and (g) 72% opening variation (OV72).

3. Results and Discussions

3.1. Validation Model Force-Displacement Curve

The displacement response of the MV-WO model aligns well with the Exp-WO in the linear portion of the graph. Conversely, the MV-WS model demonstrates lower performance than Exp-WS within the linear range but exhibits greater strength as it approaches its maximum displacement. The structural capacity of the perforated wall in MV-WO remains inferior to that of MV-WS. Although the MV-WO model incorporates higher concrete compressive strength and additional reinforcement around the opening, these enhancements were insufficient to fully compensate for the strength loss caused by

Edelweiss Applied Science and Technology
ISSN: 2576-8484
Vol. 9, No. 8: 1084-1098, 2025
DOI: 10.55214/2576-8484.v9i8.9555

the opening. The curve from the validation model shows a strong resemblance to that of the experimental model, suggesting that the layered shell element effectively captures the linear response of shear walls, but its accuracy diminishes in representing the nonlinear behavior.

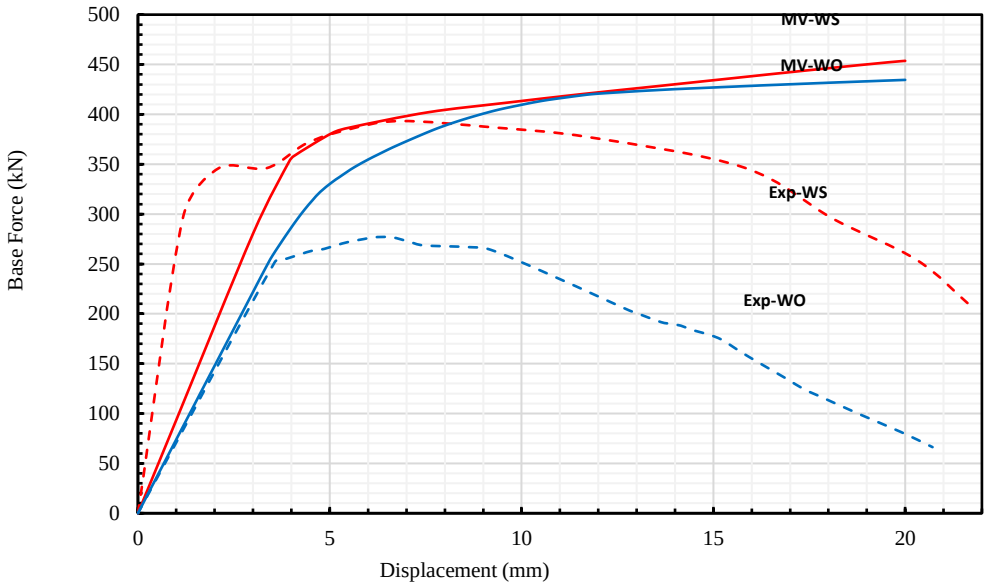

Figure 4.
The Relationship Curve of Shear Force and Displacement in the Validation Model and Experimental Test Results.

3.2. Variation Model Force-Displacement Curve

Figure 5 presents the load-displacement curves for variation models with different opening percentages, plotted on a Cartesian graph with a maximum displacement of 25 mm and a load cap of 900 kN. In comparison, Figure 6 illustrates the load-displacement curves for models with varied opening positions.

From Figure 5, it is evident that as the percentage of openings decreases, the wall's capacity to resist base shear improves when assessed in terms of displacement. At a 10 mm displacement, OV37 exhibits 30% less shear strength than OV22. OV52 shows a complete (100%) loss of strength compared to OV22, while OV72 demonstrates a dramatic reduction in strength by approximately 655% relative to OV22.

Edelweiss Applied Science and Technology
ISSN: 2576-8484
Vol. 9, No. 8: 1084-1098, 2025
DOI: 10.55214/2576-8484.v9i8.9555

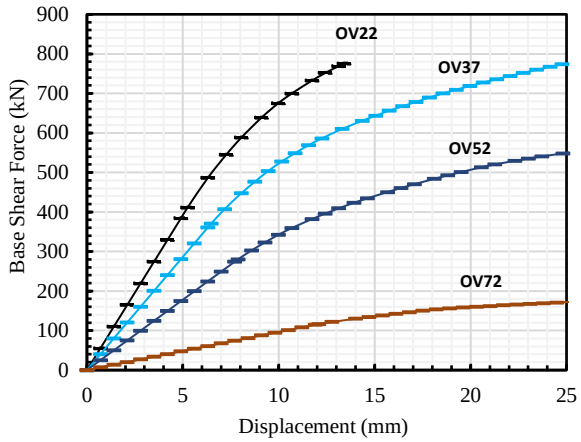

Figure 5.
Force-Displacement Curve of All Variation Models.

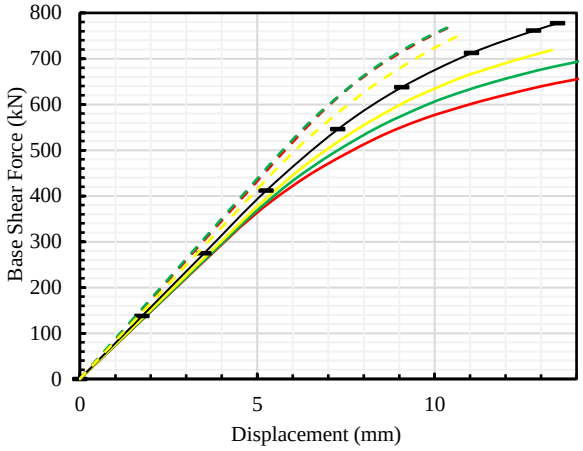

Figure 6.
Force-Displacement Curve of All Variation. Models.

Figure 6 shows that for shear walls experiencing lateral loads from the left side, a more eccentric opening position tends to enhance the wall's capacity to resist base shear. At a 10 mm displacement, the shear strength of L-OE36 is only 0.2% less than that of L-OE54. In comparison, L-OE18 has 6% lower strength, and OS (a centered opening) demonstrates a 12% reduction in strength relative to L-OE54.

On the other hand, when the lateral load is applied from the right side, increasing the eccentricity of the opening reduces the wall's resistance to base shear. At 10 mm displacement, R-OE18 has 8.2% lower shear strength than OS, R-OE36 is 13.7% lower, and R-OE54 shows an 18.6% decline in strength compared to OS.

3.3. Structural Failure Modes

3.3.1. Wall Solid Validation Model (MV-WS)

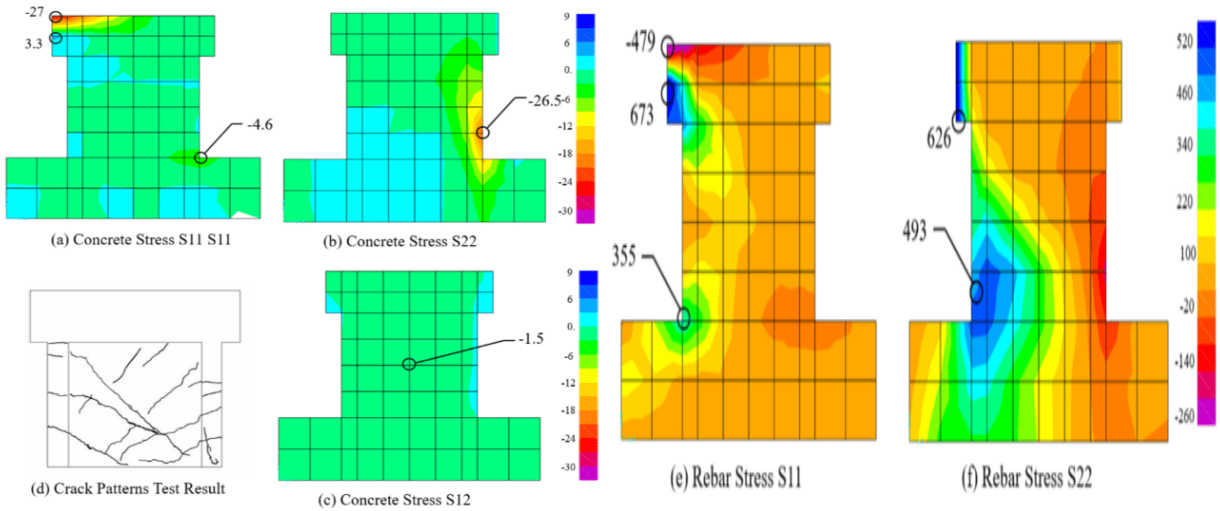

Figure 7.
MV-WS Stress Contour (MPa).

Based on the experimental results, the first crack formed at the top of the column at a drift ratio of 0.4%. As the displacement increased, horizontal cracks began to appear in the column, extending

Edelweiss Applied Science and Technology
ISSN: 2576-8484
Vol. 9, No. 8: 1084-1098, 2025
DOI: 10.55214/2576-8484.v9i8.9555

towards the end of the web. Several smaller cracks with similar inclinations also formed and spread across the web. The crack pattern in the web at peak load and at failure is shown in Figure 7d. Failure occurred due to concrete crushing at both ends of the column as a result of reversed cyclic displacement.

Based on the analysis of the full wall validation model (MV-WS), the initial crack occurred in the web at step 2, with a displacement of 1.1 mm and a force of 103 kN when the S12 stress (-1.5 MPa) exceeded its shear capacity v_c (±0.84 MPa), as shown in Figure 7c. The next crack appeared in the column at step 10, with a displacement of 8.8 mm and a force of 408 kN, when the S22 stress (-24.1 MPa) exceeded the compressive strength f_c' (24 MPa), as depicted in Figure 7b. Additionally, a crack formed at the corner of the top beam at step 15, with a displacement of 14.3 mm and a force of 432 kN when the S11 stress (3.1 MPa) surpassed its tensile capacity f_t (3.1 MPa), as shown in Figure 7a.

The experiment conducted by Sivaguru and Rao [3] did not include an assessment of the tensile strength of the reinforcing steel in the concrete section. Therefore, in this study, a tensile strength test of the reinforcing steel was performed to determine the strength of the longitudinal and transverse reinforcements, as shown in Figures 7e and 7f.

Based on the analysis of the full shear wall validation model (MV-WS), initial cracking occurred in the web section at step 2, with a displacement of 1.1 mm and a base shear force of 103 kN. This happened when the S12 shear stress (-1.5 MPa) exceeded the shear capacity of ±0.84 MPa, as illustrated in Figure 7c. Subsequent cracking was observed in the column at step 10, with a displacement of 8.8 mm and a force of 408 kN, where the S22 compressive stress (-24.1 MPa) surpassed the concrete compressive strength fy of 24 MPa, as shown in Figure 7b. Additional cracking occurred at the upper beam corner at step 15, with a displacement of 14.3 mm and a force of 432 kN, when the S11 tensile stress (3.1 MPa) reached the tensile strength f_t of 3.1 MPa, as illustrated in Figure 7a.

Regarding reinforcement behavior, the transverse reinforcement yielded at the left end of the top beam during step 17, with a displacement of 16.5 mm and a force of 440 kN. This occurred when the S11 stress reached 520 MPa, exceeding the yield strength fy of 519 MPa, as shown in Figure 7e. S22 stress data for the transverse reinforcement is not presented, as this reinforcement does not resist S22 stresses.

Meanwhile, the longitudinal reinforcement yielded at the lower left corner of the web at step 6, with a displacement of 4.4 mm and a force of 370 kN. The S22 stress in this region reached 524 MPa, surpassing the yield strength fy of 519 MPa, as shown in Figure 7f. S11 stress data is not provided for the longitudinal reinforcement, since it does not resist S11 stresses.

3.3.2. Model Validation Wall Opening (MV-WO)

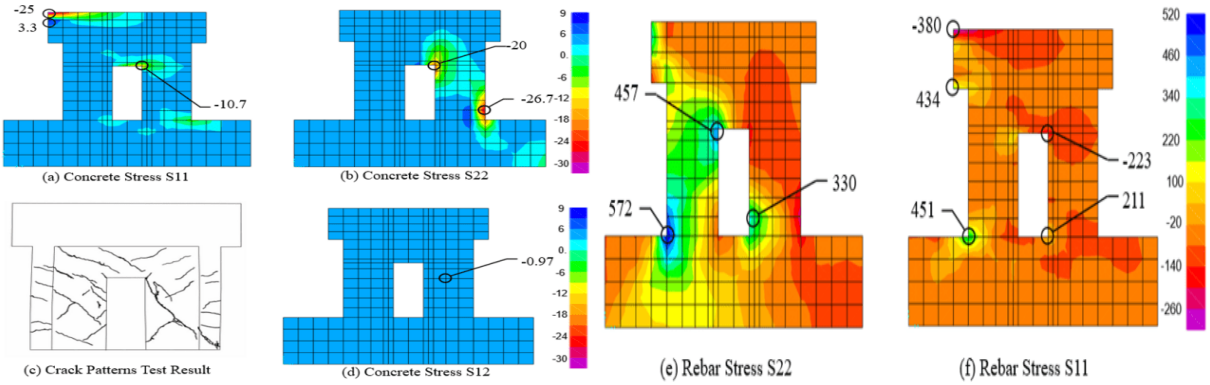

Figure 8.
MV-WO Stress Contour (MPa).

Edelweiss Applied Science and Technology
ISSN: 2576-8484
Vol. 9, No. 8: 1084-1098, 2025
DOI: 10.55214/2576-8484.v9i8.9555

Based on experimental observations, the first crack in the wall with opening (Exp-WO) initiated at the upper corner of the utility opening at a 0.2% drift ratio, propagating diagonally toward the wall's top corner. With increased lateral load, additional cracks formed near the column ends and extended toward the opening's top corner (Figure 8d).

In the corresponding validation model (MV-WO), the initial crack appeared in the web at step 1 (1 mm displacement, 103 kN force) when the S12 stress (-0.97 MPa) exceeded the shear capacity (±0.87 MPa) (Figure 8c). Cracking then occurred in the column at step 7 (6.8 mm, 370 kN) as S22 stress (-26.7 MPa) surpassed fy (26 MPa) (Figure 8b), followed by cracking at the top beam corner at step 15 (14.3 mm, 432 kN) when S11 stress (3.3 MPa) exceeded the tensile limit ft (3.37 MPa) (Figure 8a).

For reinforcement, longitudinal bars yielded at the lower-left column corner at step 4 (3.5 mm, 258 kN) with S22 stress of 572 MPa exceeding fy (519 MPa) (Figure 8e). Transverse bars, however, did not yield by the final step (20 mm, 435 kN), as the S11 stress reached only 451 MPa—still below the yield strength (Figure 8f).

3.3.3. Opening Variation 22% (OV22)

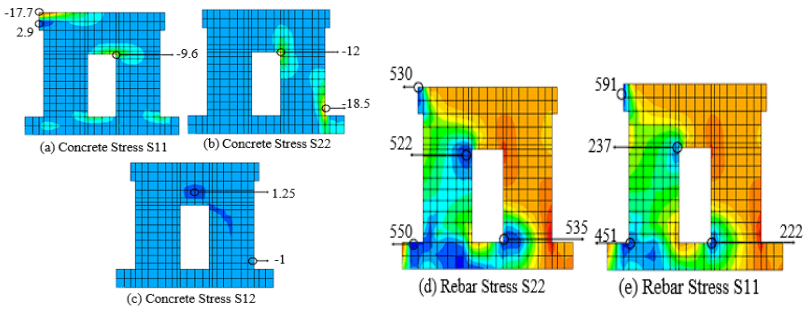

Figure 9.
OV22 Stress Contour (MPa).

From the analysis of the central opening model (OS) shown in Figure 9, the first cracks were detected in the web and column at step 3, when the displacement reached 5.3 mm and the applied force was 411 kN. At this stage, the S12 shear stresses (1.25 MPa and -1 MPa) surpassed the shear capacity vc (±0.87 MPa), as illustrated in Figure 9c. At the maximum step (step 8), with a displacement of 13.5 mm and a force of 777 kN, no new cracks were observed since the S22 compressive stress (-18.5 MPa) remained below the concrete compressive strength fy (26 MPa), as shown in Figure 9b.

In terms of reinforcement performance, the longitudinal bars experienced greater stress than the transverse bars. Yielding occurred in the longitudinal reinforcement at step 8, where the S22 stress exceeded the yield strength fy (519 MPa). Meanwhile, the transverse reinforcement did not yield at step 5, as the S11 stress remained below the same yield threshold.

Edelweiss Applied Science and Technology
ISSN: 2576-8484
Vol. 9, No. 8: 1084-1098, 2025
DOI: 10.55214/2576-8484.v9i8.9555

3.3.4. Opening Variation 37% (OV37)

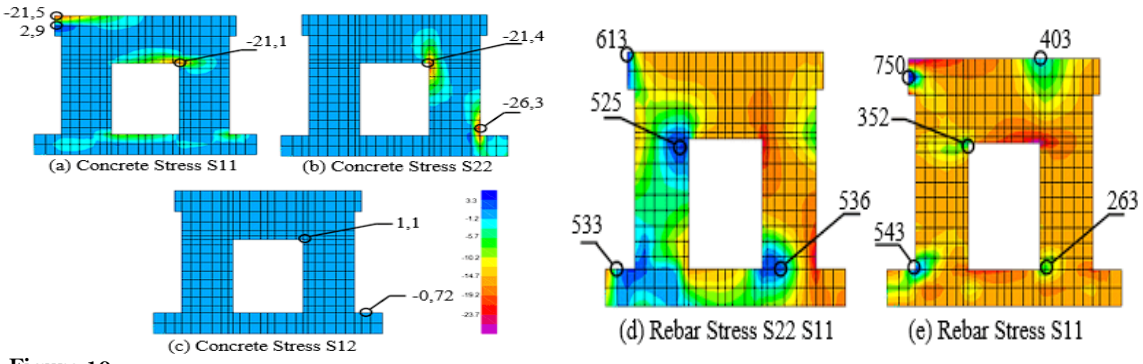

Figure 10.
OV37 Stress Contour (MPa).

From the analysis of the 37% opening variation model (OV37) in Figure 10, the initial cracking occurred in the web and column at step 3, when the structure experienced a displacement of 3.7 mm and a load of 212 kN. At this stage, the S12 shear stress (1.1 MPa) exceeded the shear strength vc (±0.87 MPa), as seen in Figure 10c. Additional cracking appeared at the final loading step (step 20), with a displacement of 24.7 mm and a load of 773 kN, where the S22 compressive stress (-26.3 MPa) surpassed the concrete compressive strength f'c (26 MPa), as indicated in Figure 10b. Meanwhile, the S11 tensile stress on the top beam (2.9 MPa) remained below the tensile strength f_t(3.3 MPa), as shown in Figure 10a.

Regarding reinforcement behavior, the longitudinal steel at the corner of the opening yielded at step 11, when the displacement reached 13.9 mm and the force was 621 kN. At this point, the S22 stress (525 MPa) exceeded the yield strength fy (519 MPa), as shown in Figure 10d.

The transverse reinforcement yielded at step 20 in both the top and bottom beams, with a displacement of 24.7 mm and a force of 773 kN. The S11 stresses in these reinforcements (750 MPa and 543 MPa) exceeded the yield strength fy, as shown in Figure 10e.

3.3.5. Opening Variation 52% (OV52)

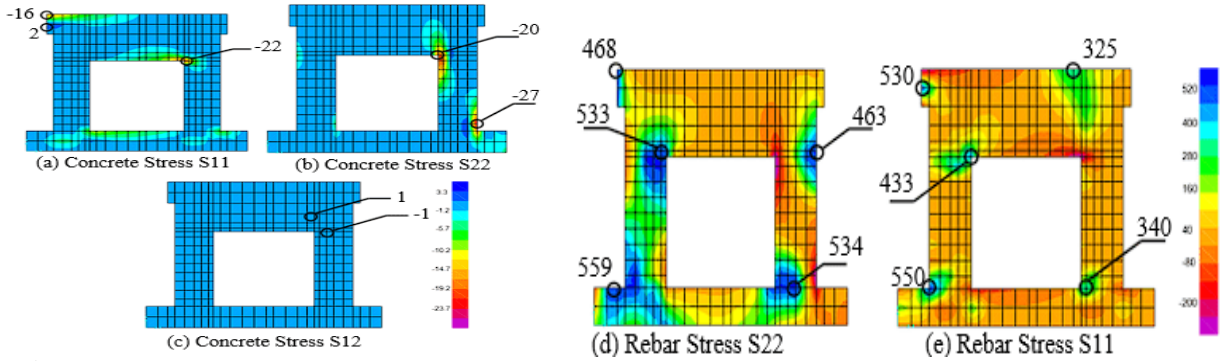

Figure 11.
OV52 Stress Contour (MPa).

Based on the analysis of OV52, initial cracks occurred at two points near the opening at step 3, with a displacement of 5.2 mm and a force of 187 kN, where the S12 stresses (1 MPa and -1 MPa) exceeded the shear capacity v_c (±0.87 MPa), as shown in Figure 11c. Further cracing occurred in the column at step 14, with a displacement of 28.8 mm and a force of 572 kN, where the S22 stress (-27 MPa)

Edelweiss Applied Science and Technology
ISSN: 2576-8484
Vol. 9, No. 8: 1084-1098, 2025
DOI: 10.55214/2576-8484.v9i8.9555

surpassed the compressive strength f_c' (26 MPa), as shown in Figure 11b. No cracks were observed at the maximum step 18, with a displacement of 35 mm and a force of 591 kN, where the S11 stress (2 MPa) did not exceed the tensile capacity f_t (3.3 MPa), as shown in Figure 11a

Based on the analysis of OV52, the longitudinal reinforcement reached the yielding condition at the opening corner at step 11, with a displacement of 20.8 mm and a force of 515 kN, where the S22 stress (533 MPa) exceeded f_y (519 MPa), as shown in Figure 11d.

The analysis results of OV52 show that the transverse reinforcement reached the yielding condition in both the top and bottom beams at step 15, with a displacement of 30.5 mm and a force of 578 kN. At this point, the S11 stresses (530 MPa and 550 MPa) exceeded f_y (519 MPa), as shown in Figure 11e.

3.3.6. Opening Variation 72% (OV72)

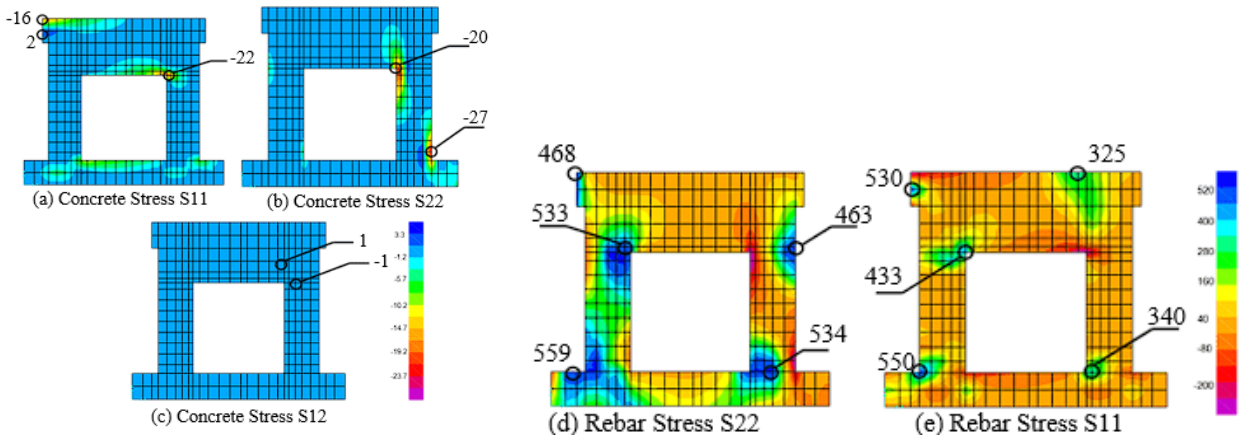

Figure 12.
OV72 Stress Contour (MPa).

Based on the analysis of OV72, initial cracking occurred near the opening at step 5, with a displacement of 7.6 mm and a force of 232 kN, where the S12 stress (-0.93 MPa) exceeded the shear capacity v_c (±0.87 MPa), as shown in Figure 12c. No cracks were observed in the web at the maximum step 19, with a displacement of 24.8 mm and a force of 172 kN, where the S22 stress (-14.7 MPa) did not exceed the compressive strength f_c' (-26 MPa), as shown in Figure 12b. Additionally, no cracks were observed at the maximum step where the S11 stress (0.6 MPa) did not exceed the tensile capacity f_t (3.3 MPa), as shown in Figure 12a.

Based on the OV72 analysis, the longitudinal reinforcement reached the yield condition at the opening corner at step 10, with a displacement of 13.3 mm and a force of 126 kN, where the stress S22 (541 MPa) exceeded f_y (519 MPa), as shown in Figure 12d.

The OV72 analysis also indicated that the transverse reinforcement reached the yield condition in the upper beam at step 15, with a displacement of 21 mm and a force of 162 kN, where the stress S11 (530 MPa) exceeded f_y (519 MPa), as shown in Figure 12e.

Edelweiss Applied Science and Technology
ISSN: 2576-8484
Vol. 9, No. 8: 1084-1098, 2025
DOI: 10.55214/2576-8484.v9i8.9555

3.3.7. Wall Loaded to the Right with 18% Eccentricity (L-OE18)

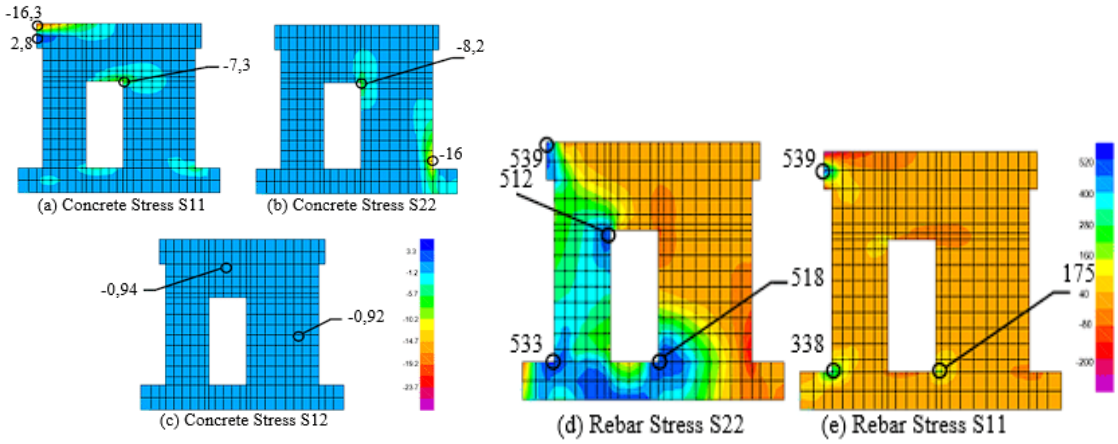

Figure 13.
L-OE18 Stress Contour (MPa).

Based on the analysis of L-OE18, initial cracking occurred in the web near the opening at step 8, with a displacement of 4.3 mm and a force of 358 kN, where the stress S12 (-0.94 MPa) exceeded v_c(±0.87 MPa), as shown in Figure 13c. No cracks were observed at the maximum step 19, with a displacement of 10.8 mm and a force of 754 kN, where the stress S22 (-16 MPa) did not exceed f_c' (-26 MPa), as shown in Figure 13b. Additionally, no cracks were observed at the maximum step where the stress S11 (2.8 MPa) did not exceed f_t (3.3 MPa), as shown in Figure 13a.

Based on the analysis of L-OE18, the longitudinal reinforcement did not reach the yield condition at the maximum step 19, with a displacement of 10.8 mm and a force of 754 kN, where the stress S22 in the web (512 MPa) did not exceed f_y (519 MPa), as shown in Figure 13d.

Based on the analysis of L-OE18, the transverse reinforcement reached the yield condition at the top beam during the maximum step 13, with a displacement of 7.4 mm and a force of 589 kN, where the stress S11 (539 MPa) exceeded f_y (519 MPa), as shown in Figure 13e.

3.3.8. Wall Loaded to the Right with 36% Eccentricity (L-OE36)

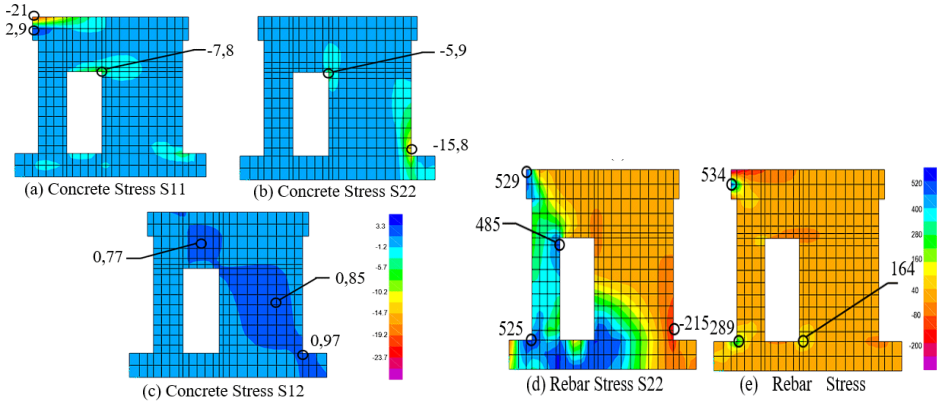

Figure 14.
L-OE36 Stress Contour (MPa).

Edelweiss Applied Science and Technology
ISSN: 2576-8484
Vol. 9, No. 8: 1084-1098, 2025
DOI: 10.55214/2576-8484.v9i8.9555

Based on the analysis of L-OE36, initial cracking occurred in the column at step 8 with a displacement of 4.2 mm and a force of 371 kN, where the stress S12 (0.97 MPa) exceeded v_c (±0.87 MPa), as shown in Figure 14c. No cracks were observed at the maximum step 20, with a displacement of 10.5 mm and a force of 774 kN, where the stress S22 (-15.8 MPa) did not exceed f_c' (-26 MPa), as shown in Figure 14b. Additionally, no cracks were observed at the maximum step where the stress S11 (2.9 MPa) did not exceed f_t (3.3 MPa), as shown in Figure 14a.

Based on the analysis of L-OE36, the longitudinal reinforcement reached the yield condition at the maximum step 20 with a displacement of 10.5 mm and a force of 774 kN, where the stresses S22 in the top and bottom beams (529 MPa and 525 MPa) did not exceed f_y (519 MPa), as shown in Figure 14d.

Based on the analysis of L-OE36, the transverse reinforcement reached the yield condition at the top beam during step 13 with a displacement of 6.8 mm and a force of 584 kN, where the stress S11 (534 MPa) exceeded f_y (519 MPa), as shown in Figure 14e.

3.3.9. Wall Loaded to the Right with 54% Eccentricity (L-OE54)

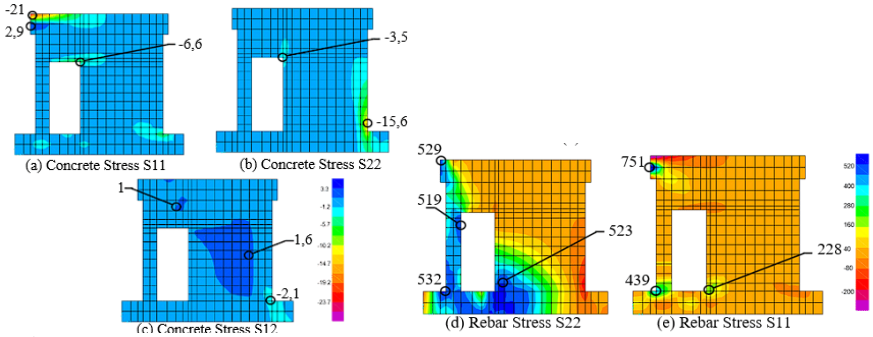

Figure 15.
L-OE54 Stress Contour (MPa).

3.3.10. Wall Loaded to the Left with 18% Eccentricity (R-OE18)

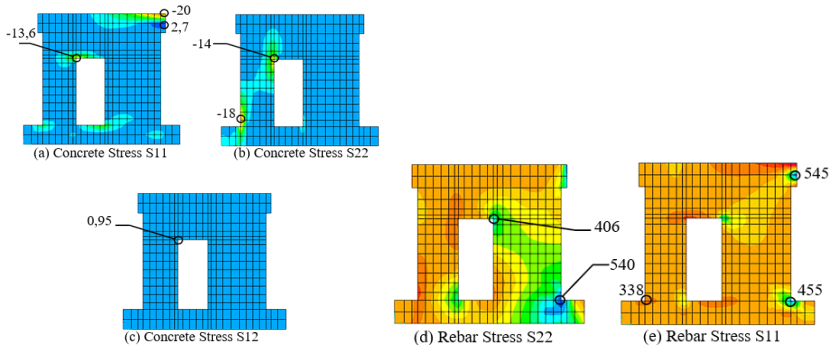

Figure 16.
R-OE18 Stress Contour (MPa).

Based on the analysis of R-OE18, initial cracking occurred in the web near the opening at step 5 with a displacement of 3.3 mm and a force of 251 kN, where the stress S12 (0.95 MPa) exceeded v_c (±0.87 MPa), as shown in Figure 16c. No cracks were observed at step 19 with a maximum displacement of 13.3 mm and a force of 719 kN, where the stress S22 (-18.7 MPa) did not exceed f_c' (-26 MPa), as shown in Figure 16b. Additionally, no cracks occurred at the maximum step where the stress S11 (2.7 MPa) did not exceed f_t(3.3 MPa), as shown in Figure 16a.

Edelweiss Applied Science and Technology
ISSN: 2576-8484
Vol. 9, No. 8: 1084-1098, 2025
DOI: 10.55214/2576-8484.v9i8.9555

Based on the analysis of R-OE18, the longitudinal reinforcement reached the yield condition at step 9 with a displacement of 5.8 mm and a force of 433 kN, where the stress S22 (540 MPa) in the lower beam exceeded f_y (519 MPa), as shown in Figure 16d.

Based on the analysis of R-OE18, the transverse reinforcement reached the yield condition at step 13 with a displacement of 5 mm and a force of 376 kN, where the stress S11 (545 MPa) in the upper beam exceeded f_y (519 MPa), as shown in Figure 16e.

3.3.11. Wall Loaded to the Left with 36% Eccentricity (R-OE36)

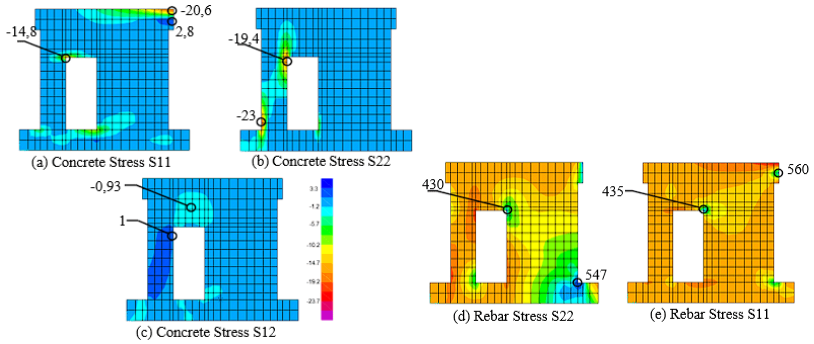

Figure 17.
R-OE36 Stress Contour (MPa).

Based on the analysis of R-OE18, the longitudinal reinforcement reached the yield condition at step 9 with a displacement of 5.8 mm and a force of 433 kN, where the stress S22 (540 MPa) in the lower beam exceeded f_y (519 MPa), as shown in Figure 17d.

Based on the analysis of R-OE36, initial cracking occurred in the web near the opening at step 5 with a displacement of 4.4 mm and a force of 328 kN, where the stress S12 (1 MPa) exceeded v_c (±0.87 MPa), as shown in Figure 17c. No cracks were observed at the maximum step 19 with a displacement of 17.7 mm and a force of 741 kN, where the stress S22 (-15.8 MPa) did not exceed f_c' (-26 MPa), as shown in Figure 17b. Additionally, no cracks were observed at the maximum step where the stress S11 (2.8 MPa) did not exceed f_t (3.3 MPa), as shown in Figure 16a.

Based on the analysis of R-OE36, the longitudinal reinforcement reached the yield condition at step 7 with a displacement of 6 mm and a force of 431 kN, where the stress S22 in the lower beam (547 MPa) exceeded f_y (519 MPa), as shown in Figure 17d.

Based on the analysis of R-OE36, the transverse reinforcement reached the yield condition in the upper beam at step 10 with a displacement of 9.8 mm and a force of 601 kN, where the stress S11 in the upper beam (560 MPa) exceeded f_y (519 MPa), as shown in Figure 17e.

Edelweiss Applied Science and Technology
ISSN: 2576-8484
Vol. 9, No. 8: 1084-1098, 2025
DOI: 10.55214/2576-8484.v9i8.9555

3.3.12. Wall Loaded to the Left with 54% Eccentricity (R-OE54)

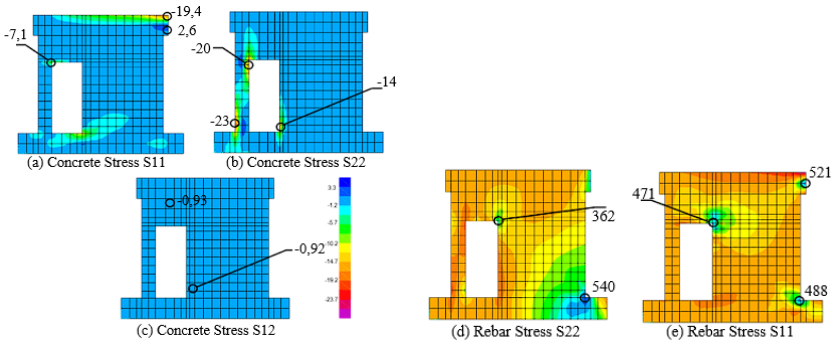

Figure 18.
R-OE54 Stress Contour (MPa).

Based on the analysis of R-OE54, the initial crack occurred in the column at step 7 with a displacement of 5.4 mm and a force of 390 kN, where the stress S12 (-0.93 MPa) exceeded v_c(±0.87 MPa), as shown in Figure 18c. No cracks were observed at the maximum step 19 with a displacement of 17.7 mm and a force of 699 kN, where the stress S22 (-23 MPa) did not exceed f_c' (-26 MPa), as shown in Figure 18b. Additionally, no cracks were observed at the maximum step where the stress S11 (2.8 MPa) did not exceed f_t (3.3 MPa), as shown in Figure 18a.

Based on the analysis of R-OE54, the longitudinal reinforcement reached the yield condition in the web at step 7 with a displacement of 5.4 mm and a force of 390 kN, where the stress S22 in the lower beam (540 MPa) exceeded f_y (519 MPa), as shown in Figure 18d.

Based on the analysis of OE54, the transverse reinforcement reached the yield condition in the upper beam at step 12 with a displacement of 6.7 mm and a force of 572 kN, where the stress S11 (521 MPa) exceeded f_y (519 MPa), as shown in Figure 18e.

4. Conclusion and Recommendation

This research modeled the nonlinear behavior of reinforced concrete shear walls with openings using SAP2000. Two validation models—MV-WS and MV-WO—were analyzed, and the modeling approach was verified by comparing the resulting P-Δ curves and crack patterns with those from experiments (Exp-WS and Exp-WO), showing a strong correlation. Following validation, eight additional models were developed: four with varying opening percentages (OV22, OV37, OV52, and OV72), and four with different opening positions (OS, OE18, OE36, and OE54).

The use of layered shell elements in SAP2000 proved effective for simulating the elastic behavior of shear walls, although it showed limitations in accurately representing plastic behavior. SAP2000's capacity to model cracked shear walls does not fully replicate real-world conditions. The analysis results indicate that smaller opening percentages improve the wall's ability to withstand base shear forces. Furthermore, in models subjected to right-side lateral loads, greater eccentricity in the opening position increases shear resistance. However, under left-side lateral loads, increased eccentricity reduces the wall's capacity to resist base shear.

Transparency:

The authors confirm that the manuscript is an honest, accurate, and transparent account of the study; that no vital features of the study have been omitted; and that any discrepancies from the study as planned have been explained. This study followed all ethical practices during writing.

Edelweiss Applied Science and Technology
ISSN: 2576-8484
Vol. 9, No. 8: 1084-1098, 2025
DOI: 10.55214/2576-8484.v9i8.9555

Acknowledgments:
This study was conducted as part of the undergraduate program in Civil Engineering, Faculty of Engineering, Udayana University. The authors gratefully acknowledge the academic environment and institutional support that enabled the completion of this research.

References

[1] M. Rezapour and M. Ghassemieh, "Macroscopic modelling of coupled concrete shear wall," *Engineering Structures*, vol. 169, pp. 37-54, 2018. https://doi.org/10.1016/j.engstruct.2018.04.088

[2] N. Haghi, S. Epackachi, and M. Taghi Kazemi, "Macro modeling of steel-concrete composite shear walls," *Structures*, vol. 23, pp. 383-406, 2020. https://doi.org/10.1016/j.istruc.2019.10.018

[3] V. Sivaguru and G. A. Rao, "Strength and behavior of reinforced concrete squat shear walls with openings under cyclic loading," *ACI Structural Journal*, vol. 118, no. 5, pp. 235–50, 2021. https://doi.org/10.14359/51732832

[4] D. W. Kelly, P. Hsu, and M. Asudullah, "Load paths and load flow in finite element analysis," *Engineering Computations*, vol. 18, no. 1-2, pp. 304-313, 2001. https://doi.org/10.1108/02644400110365923

[5] I. Computers and Structures, *Structural analysis program, Ver. 25.0.0*. Berkeley (CA): Computers and Structures, Inc, 2017.

[6] Badan Standardisasi Nasional (BSN), *Earthquake resistance planning procedures for building and non-building structures*. Jakarta (ID): BSN, 2019.

[7] Applied Technology Council (ATC), *Seismic evaluation and retrofit of concrete buildings (ATC 40)*. Sacramento (CA): California Seismic Safety Commission, 1996.

[8] RJPotteiger, "Monolithic concrete in construction [Internet]," 2023. https://www.rjpotteigerinc.com/blog/monolithic-concrete-construction/

[9] R. Cook, *Finite element modeling for stress analysis*. New York (NY): John Wiley & Sons, 1995.

[10] A. Vatanshenas, "Nonlinear analysis of reinforced concrete shear walls using nonlinear layered shell approach," *Nordic Concrete Research*, vol. 65, no. 2, pp. 63-79, 2021. https://doi.org/10.2478/ncr-2021-0014